

On the Capacitance Spectroscopy of $\text{Cu}_2\text{ZnSnS}_4$ Typed Solar Cells Anisotype Heterojunction by SCAPS-1D

Olusola Akinrinola*+, Ayodeji Awodugba**, Momodu Jain**, Mojinyinola Awodele*,
Omowunmi Akinrinola*, Abideen Ibiyemi***

* Department of Pure and Applied Physics, Faculty of Pure and Applied Sciences, Ladoke Akintola University of Technology, P.M.B 4000, Ogbomoso, Nigeria

** Department of Physics, Division of Physical and Natural Sciences, P.M.B 3530, Banjul, Gambia

*** Department of Physics, Faculty of Sciences, Federal University Oye-Ekiti, Nigeria

(oakinrinola@pgschool.lautech.edu.ng, aoawodugba@lautech.edu.ng, mkawodele@lautech.edu.ng, whygbedu@gmail.com,
abideen.ibiyemi@fuoye.edu.ng)

+ Corresponding Author; Akinrinola Olusola, Department of Pure and Applied Physics, Ladoke Akintola University of Technology, P.M.B 4000, Ogbomoso, Nigeria, +234739536379, oakinrinola@pgschool.lautech.edu.ng

Received: 07.10.2019 Accepted: 28.01.2021

Abstract - One of the most reliable renewable energy source is the solar energy from the sun. However, most materials have been unable to meet their potentials as a good absorber layer in thin films. Most recently, $\text{Cu}_2\text{ZnSnS}_4$ (CZTS) have been identified as a good absorber layer, yet the same problem persists. In this study, we examined the depletion capacitance vis-a-vis the voltage and range of frequencies based on heterojunction types and structures. The modeled solar cell consisted three types of materials used as buffer layer (BL) (ZnO:Al (AZO), In_2S_3 (IS) and $\text{CH}_3\text{NH}_3\text{PbCl}_3$ (PVKT)). The band gap model of n/n/p anisotype heterojunction for the three BLs were constructed from the obtained data of the simulated solar cells. The band offsets ΔE_C and ΔE_V in electron-volts at n/n for AZO, IS and PVKT are; 0.07071 and 0.18794, 0.09768 and 0.72367 and 0.67541 and 2.54541 respectively. Also, at n/p ΔE_C and ΔE_V for AZO, IS and PVKT are; 0.14251 and 1.93251, 0.49011 and 1.73011 and 0.34041 and 1.73920 respectively. Based on the trivial AC signal that was superimposed on the dc biased charges, AZO and IS shows an exponential response of the capacitance reliance on the voltage across the depletion region. The Capacitance spectroscopy of this solar cell showed that anisotype heterojunction may be manipulated to make use of the voltage reliance on junction capacitance when the need to electronically vary it arises.

Keywords: Solar cells; Anisotype; Heterojunction; Band offsets; Capacitance, CZTS

1. Introduction

Solar cells are photovoltaic devices (transducers) that converts the electromagnetic radiation from the Sun (solar energy - the most important renewable energy sources) into utilizable electrical energy. The conversion process of sun-radiation to electrical energy is a sequence of four basic steps [1]; (i) Light absorption that causes a transition from a ground state, (ii) the conversion of the excited state into at least one free electron-hole pair(photo-generation), (iii) the presence of asymmetric forces in the device such that the produced free electron travel in one direction and the

produced free holes travel in the opposite direction (separation) and (iv) completion of an external circuit by the combination of the returning electrons with holes to return the absorber to the ground state (non-equilibrium open system).

The materials used as the absorber (i.e. ability to absorb sunlight) typify solar cells. Solar cells are classified into first, second, third generations. The first generation solar cells are sometimes referred to as; traditional or wafer based which are made from mono/poly crystalline silicon. The second generation solar cells are thin-film based which

are made from amorphous silicon, CdTe and Cu(InGa)Se₂ (CIGS). The third generation cells are new thin-film made from different configurations and sometimes referred to as emerging photovoltaics. The first and second generations are commercially important in utility scaling of photovoltaic power generation stations. The third generation is yet to be commercialized due to ongoing research on its viability [2].

The second generation have the following advantages;

(i) thinner devices that requires fewer materials and can tolerate lower-quality raw materials since charge carriers travel short distances in the semiconductor before being collected by the metallic contact [3], (ii) Crystalline silicon devices (first generation) rely on the silicon wafer itself for rigidity, while thin-film devices are typically deposited on low-cost substrates (foil/glass).

The use of photovoltaic for a substantial portion of grid connected electricity generation has its merits, which are; zero pollution energy source, decentralized power generation that will discourage sabotages and low-maintenance power plants with inexhaustible fuel supplies. In the quest for sustainable solar renewable energy, inorganic thin film solar cells (ITFSC) are at the forefront of importance. Many materials have been applied in the planar configuration to bring about a much more conversion efficiency (CE).

Cu₂ZnSnS₄ (CZTS) is used to replace CIGS as an absorber in solar cells [4]. In spite of rapid improvement in efficiency, the understanding of the operation mechanism of CZTS based solar cells, which should be the requirement for further improvement is not sufficient. When the solar cell is exposed to sunlight, there are, carrier generation, drift/diffusion and recombination.

The drift/diffusion process induces a charge variation into the solar cell which is followed by a charge in the voltage across the cell. There is no detailed report on junctions' contributions to the conversion efficiency. There are many studies on increasing the efficiency of the photovoltaic (PV) systems used as renewable energy sources as a solution for the reduction of environmental pollution. For the understanding of device physics and optimum design for efficiency enhancement, device simulation has been used widely in organic solar cells [5].

In ITFSC, Wannier-type exciton is exhibited by CZTS, as an absorber. Structural similarity and Wannier type exciton do make it important that an existing device simulator has to be used [4, 5]. In this study, SCAPS-1D developed by Mac Bulgeman and his co researchers at the University of Gents, was used to model CZTS solar cells. The validity of the device simulation in terms of conversion efficiency compared with the real device has been reported [4]. The simulation of the admittance/capacitance spectroscopy of this CZTS based solar cells in relation to conversion efficiency. Capacitance spectroscopy

techniques, as reported [6] can be used to examine defects in the p-type layer since it's a well-known fact that free carrier trapping and emission in deep defect levels will add to the capacitance of the solar cell in the p-n region [5,7]. The intrinsic defects and impurities in the absorber layer do possess an indicative effect on carrier recombination and this will invariably affect the quantum efficiency of the cell. Further optimization requires knowledge to regulate these defects.

2. Energy band theory

The energy band gaps of two different materials that come in contact to create a junction between the materials, the Fermi levels position in these two materials must coincide at thermal equilibrium. The distribution function of the donor interface (F_{SD}) is given [7] as:

$$F_{SD}(E_t) = \frac{1}{1+g e^{\left(\frac{E_F - E_t}{K_B T}\right)}} \quad (1)$$

and for acceptor interface traps (F_{SA}) as;

$$F_{SA}(E_t) = \frac{1}{1+g e^{\left(\frac{E_t - E_F}{K_B T}\right)}} \quad (2)$$

where K_B is Boltzmann constant, T is temperature, E_F is the Fermi energy, E_t is the energy of the interface trap and g is the ground state degeneracy, which is 2 for donor and 4 for acceptor.

The metal work function is determined by the disparity in energy between the vacuum level and the Fermi level. According to [7], the metal work function acts independently and the property of the semiconductor surface is fixed by the barrier height. The space charge (Q_{SC}) per unit area of the semiconductor and the depletion-layer capacitance (C) per unit area are given by:

$$Q_{SC} = q N_D W = \sqrt{2q \epsilon_s N_D \left(V_{bi} - V - \frac{KT}{q} \right)} \quad (3)$$

$$C = \frac{1}{\partial Q_{SC} / \partial V} = \frac{q \epsilon_s N_D}{2 \left(V_{bi} - V - \frac{KT}{q} \right)} = \frac{\epsilon_s}{W} \quad (4)$$

and

$$\frac{1}{C^2} = \frac{2 \left(V_{bi} - V - \frac{KT}{q} \right)}{q \epsilon_s N_D} \quad (5)$$

Where q is the electrostatic charge, N_D is the carrier concentration of the donor ϵ_s is the permittivity of the semiconductor, V is the applied voltage and V_{bi} is the built in voltage.

Differentiating equation (5) with respect to V yield:

$$\frac{d\left(\frac{1}{C^2}\right)}{dV} = \frac{2}{q \epsilon_s N_D} \quad (6)$$

Therefore:

$$N_D = \frac{2}{q \epsilon_s} \left[\frac{d\left(\frac{1}{C^2}\right)}{dV} \right]^{-1} \quad (7)$$

The implication of equation (3) is that N_D is constant throughout the depletion region, by plotting C^{-2} against V , a straight- line graph must be obtained [7, 8]. However, if N_D

is not constant, the differential capacitance method may be useful to detect the doping profile.

A doped semiconductor is either n- or p- type. The planar configuration of the solar cell in this study shows n/n/p/ junctions of n/n (homo-junction) and n/p (heterojunction), as arranged and set in Fig. 1. We assumed a model of n/n junctions to be pure resistance with n/p and p/m junctions to be combinations of capacitance and resistance. These assumptions led to the circuit network of Fig. 2. Series-parallel circuits are best solved by Admittance method by first reducing the parallel circuit to a match series circuit which are then combined to the remainder of the circuit [9].

The equivalent series impedance Z_{eq} is given as;

$$Z_{eq} = \frac{1}{\gamma_{eq}} \quad (8)$$

For Fig. 2, equivalent series Admittance (γ_{eq}) is given as;

$$\gamma_{eq} = \gamma_s + \gamma_1 + \gamma_2 \quad (9)$$

Taking each branch of the network in series (Fig. 2), consecutively, as; γ_s , γ_1 , and γ_2 and define them as;

$$\gamma_s = \frac{1}{R_s} \quad (10)$$

$$\gamma_1 = \frac{1}{R_A} + \frac{R_1}{R_1^2 + \omega^2 C_1^2} + \frac{R_2}{R_2^2 + \omega^2 C_2^2} + j \left[\frac{1}{\omega C_A} + \frac{\omega C_1}{R_1^2 + \omega^2 C_1^2} + \frac{\omega C_2}{R_2^2 + \omega^2 C_2^2} \right] \quad (11)$$

$$\gamma_2 = \frac{1}{R_C} + \frac{j}{\omega C_D} \quad (12)$$

Now, substituting equations (10), (11) and (12) into (9) gave:

$$\gamma_{eq} = \frac{1}{R_s} + \frac{1}{R_C} + \frac{1}{R_A} + \frac{R_1}{R_1^2 + \omega^2 C_1^2} + \frac{R_2}{R_2^2 + \omega^2 C_2^2} + j \left[\frac{1}{\omega C_A} + \frac{1}{\omega C_D} + \frac{\omega C_1}{R_1^2 + \omega^2 C_1^2} + \frac{\omega C_2}{R_2^2 + \omega^2 C_2^2} \right] \quad (13)$$

And by substituting equation (13) into (8), we obtained:

$$Z_{eq} = \left\{ \frac{1}{R_s} + \frac{1}{R_C} + \frac{1}{R_A} + \frac{R_1}{R_1^2 + \omega^2 C_1^2} + \frac{R_2}{R_2^2 + \omega^2 C_2^2} + j \left[\frac{1}{\omega C_A} + \frac{1}{\omega C_D} + \frac{\omega C_1}{R_1^2 + \omega^2 C_1^2} + \frac{\omega C_2}{R_2^2 + \omega^2 C_2^2} \right] \right\}^{-1} \quad (14)$$

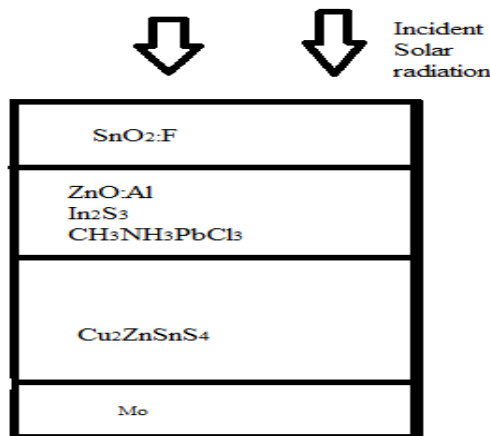


Fig. 1. The planar configuration for the CZTS based solar cell

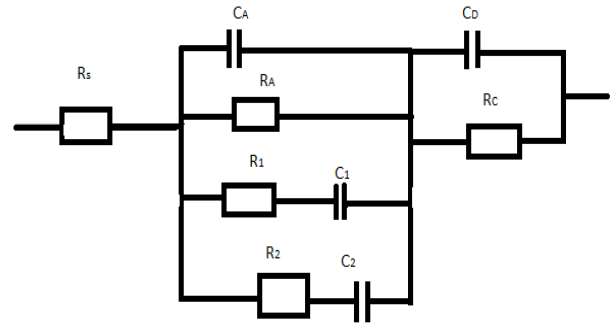


Fig. 2. The equivalent model circuit network for Fig. 1. based on planar configuration of the solar cell.

3. Methodology and Device simulation parameter

The device simulator – SCAPS-1D was used in a planar configuration as presented in Fig. 1. The simulation was done for AC (alternating current) electrical measurements, which were performed in the A.M 1.5 light condition. The solar cell consists of transparent conductive oxide (TCO)/buffer layer (BL)/CZTS/metallic hole transport layer (MHTL). The physics parameters as expressed in Table 1 for the materials involved for TCO, buffer layer, absorber, CZTS and MHTL are mainly based on SnO₂:F (FTO), BL – (ZnO:Al (AZO); In₂S₃ (IS) and CH₃NH₃PbCl₃ (PVKT)), Cu₂ZnSnS₄ (CZTS) and Mo respectively.

The buffer (BL) is often called blocking layer [5]. An interface trapped charge exists within the forbidden gap due to the interaction of the periodic lattice at heterojunction. An interface trapped is considered a donor if it can become positive through donation of an electron and as well an acceptor interface trap by accepting electron.

In this model, interface defect layer (IDL) is assumed to take into account, the interface recombination that is placed between BL/CZTS and CZTS/Mo heterojunctions layers. The basic matched model circuit for Figure 1 is as expressed in Figure 2. In the figure, C_A and C_D are the BL/CZTS and CZTS/Mo capacitances at these interface traps and R_A and R_C are the attendant resistances respectively. The branches R₁ – C₁ and R₂ – C₂ are added to the network to account for recombination sites in the CZTS.

The magnitude of each layer was taken from our report with conversion efficiency of 19.8 % which has been reported elsewhere based on the planar configuration of the same solar cell with ZnO:Al as the BL. The exact values are expressed in Table 1 for the optical and electronic parameters/properties of the materials used in the simulation [10].

4. Simulation Results and Discussions

4.1 Energy Band Structure

The band gap model of n/n/p model anisotype heterostructure for the three buffer layers (BLs); AZO, IS

and PVKT halides were constructed from the obtained data of the simulated solar cells as shown in Figure 3. Figure 3; (a) and (b) shows a quantum well with unequal barriers while Figure 3 (c) is a typical concave pseudo potential step. The Anderson's rule, which foretells the band alignment based on the attributes of vacuum-semiconductor interfaces has its limitation based on the omission of chemical attachment.

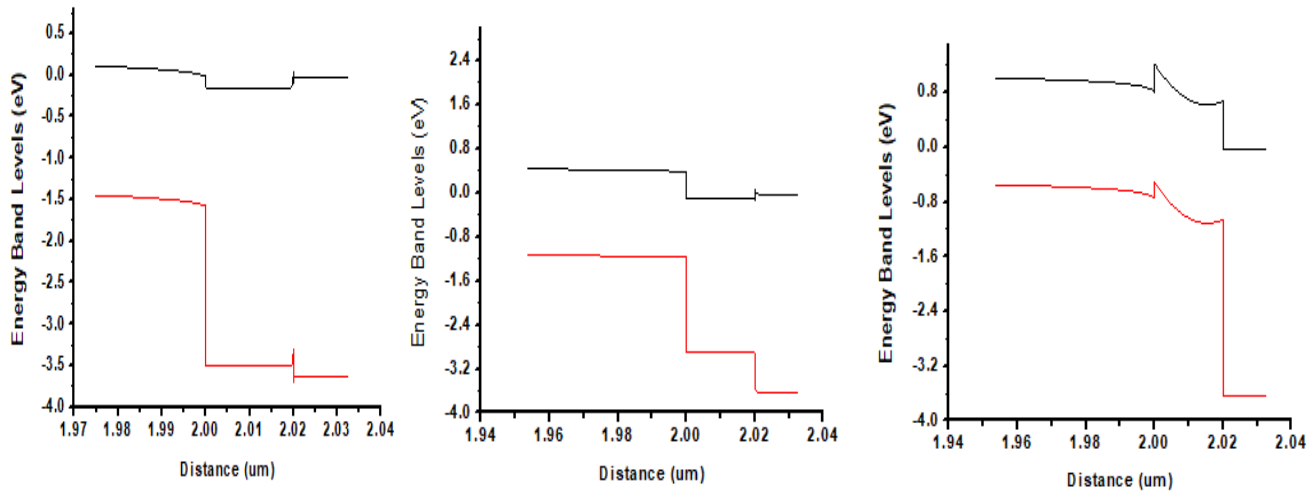
A common anion rule, which was proposed based on the valence band correlates to anionic states, in which

substance with relative anions ought to have quite small valence band offsets. This does not explain the data but gave the trend that two materials with anions that are unrelated will possess larger valence band offsets compared with the conduction band offsets. A gap state model has its basis on more familiar metal-semiconductor junctions where the conduction band offset is a replica of the disparity in the Schottky barrier height [11]. This assumption quite agrees well with systems whose two materials are closely lattice matched [12].

Table 1: Opto-electronic properties of the materials used in the simulation

Parameters	p-CZTS	n-FTO	n-AZO	n-In ₂ S ₃	n-CH ₃ NH ₃ PbCl ₃
Thickness (nm)	2.0 x 10 ³	12.5	20	20	20
Relative permittivity	10	10	9	13.5	6.5
Electron affinity (eV)	4.21	4.50	4.35	4.7	3.8
Band gap Eg (eV)	1.56	3.60	3.35	2.8	1.73
Density of states– conduction band Nc (cm ⁻³)	2.2 x 10 ¹⁸	1.2 x 10 ²⁰	2.2 x 10 ¹⁸	1.8 x 10 ¹⁹	2.2 x 10 ¹⁷
Density of states – valence band Nv (cm ⁻³)	1.8 x 10 ¹⁹	7.0 x 10 ²⁰	1.8 x 10 ¹⁹	4.0 x 10 ¹³	1.8 x 10 ¹⁹
Electron mobility (cm ² V ⁻¹ s ⁻¹)	100	20	25	400	0.2
Hole mobility (cm ² V ⁻¹ s ⁻¹)	20	100	100	210	0.2
Donor concentration (cm ⁻³)	0	3.5 x 10 ²⁰	1.0 x 10 ¹⁸	1.0 x 10 ¹⁷	1.8 x 10 ¹⁸
Acceptor concentration (cm ⁻³)	4.0 x 10 ¹⁶	0	0	10	0
Gaussian defect density	1.0 x 10 ¹²	1.0 x 10 ¹⁸	1.0 x 10 ¹⁸	1.0 x 10 ¹⁸	1.0 x 10 ¹⁸

Fig. 3. Energy Band diagram of (a) CZTS/AZO/FTO (b) CZTS/IS/FTO (c) CZTS/PVKT/FTO



Schottky barrier height [11]. This assumption quite agrees well with systems whose two materials are closely lattice matched [12]. The band alignments at n/n and n/p for the materials; AZO, IS and PVKT are Type I (straddling gap) and Type II (staggered gap), Type I (straddling gap) and Type II (staggered gap) and Type II and Type II at both interfaces for each of the BLs respectively. The basic technique for determining band offsets are by deducing them from exciton's energies in the luminescence spectra.

The values of band offsets ΔE_C and ΔE_V at n/n and n/p are for AZO, IS and PVKT are reported in Table 2.

Table 2: The values of band offsets at n/p and n/n interfaces

B L	n/p		n/n	
	ΔE_C (eV)	ΔE_V (eV)	ΔE_C (eV)	ΔE_V (eV)
AZO	0.14251	1.93251	0.07071	0.18794
IS	0.49011	1.73011	0.09768	0.72367
PVKT	0.34041	1.73920	0.67541	2.54541

There is however little information on how CZTS performs as part of a thin film stack and the role of different material layers that will contribute to the diffusion capacitance within the depletion width. One can predict at this junction that the band discontinuities at each of the junction and thickness of each materials plays a vital role in the size of the capacitance therein.

The continuous density of states distribution with interface states may be theoretically study to examine the electrical conduction in semiconductor anisotype heterojunction [7]. The defect states are reported in their density of states function and recombine cross sections for transitions to the valence and conduction bands.

4.2 Capacitance Voltage Measurement

The depletion width at an abrupt anisotype heterojunction plays a vital role in the capacitance of such device. A trivial AC signal was superimposed on a dc biased charge of one sign were induced on the P- side and the charges of opposite sign in the n- side. The relationship between the capacitance and voltage were given in Fig. 4 for the three BLs. AZO and IS shows an exponential response of the capacitance with the voltage across the depletion region. The PVKT shows a continuous rough linear relationship with a sudden increase between 0.6 and 0.7 V.

The inverse of the reactance of the capacitance (Admittance) was taken when a trivial AC signal is applied and the conductance aspect of the Admittance was plotted against the applied AC voltage and the result was given in Fig. 5.

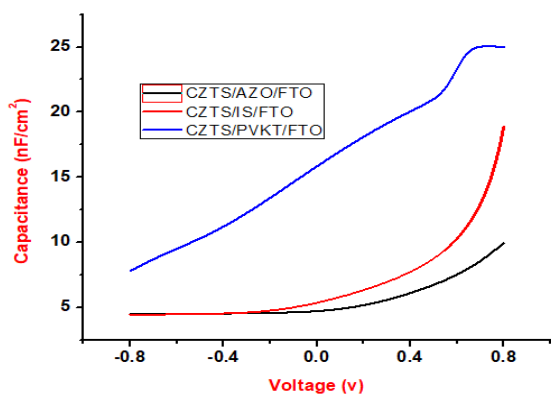


Fig. 4. Capacitance – Voltage profiling of CZTS with different BLs

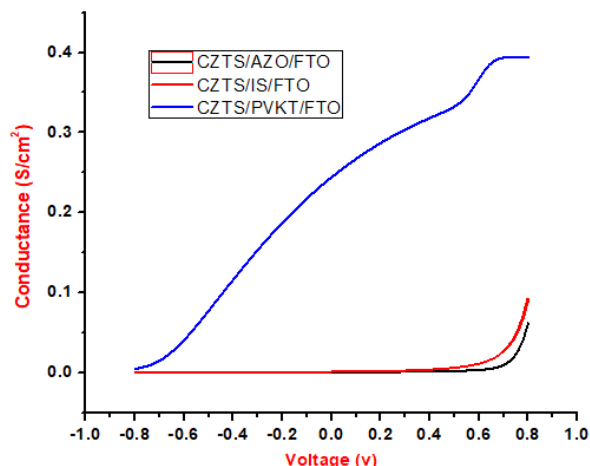


Fig. 5. Conductance – Voltage profiling of CZTS with different BL

This equally shows that the conductance (the real part of admittance), exponentially grow with the applied voltage in AZO and IS, the PVKT as well gave a continuous rough linear relationship with the same sudden increase between 0.6 and 0.7 V.

The Mottschottky plot (MSP) for these models was plotted (i.e. C^{-2} against Voltage) as expressed in Fig 6. This is calculated by approximating the curve locally by a very low order polynomial. The point in local neighborhood was three (a part, 1 left and 1 right neighbor). The polynomial order in the middle of the range is of order two (best second order parabola through neighbor points). Also, the polynomial order at the edges of the range is one (best straight line through neighbor points).

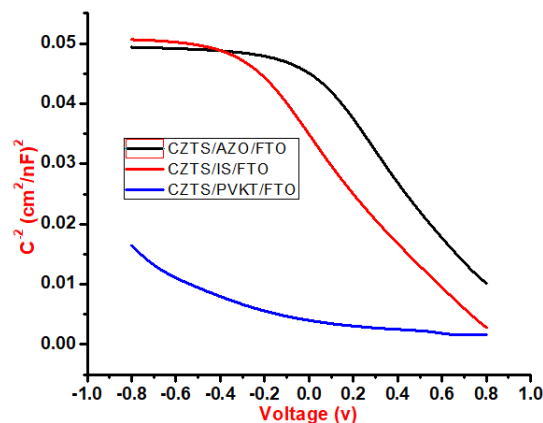


Fig. 6. Mottschottky profiling of CZTS with different BLs.

The Helmholtz capacitance, potential doping density or flat band is the system properties that may be deduced from MSP. It is necessary to note that the slope supposed to give the doping density since the dielectric is a known constant for each of the BLs.

The built in potential is deduced from intercepts to the x-axis and allows the establishing of the reference of potential with respect to the conduction band. The depletion width is dependent upon the applied voltage which thus presents information on the BLs internal properties such as its doping profile and defect densities that is electrically active as presented in Figure 7 (a) and (b).

All these plots were necessary to understand how the capacitance varies with the voltage through the depletion width. The anisotype heterojunction can be manipulated to make use of the voltage dependence junction capacitance. This is applicable where a device whose capacitance is needed to be varied electronically rather than mechanical.

4.3 Capacitance frequency Measurement

The capacitance – frequency measurement can be used to fix the impedance of the solar cell. As expressed in Figs. 8, the capacitance gave a constant capacitance over a range of frequencies for both AZO and IS BLs but an exponential decrease over the same wide range of frequencies for PVKT as a BL.

The conductance (Admittance’s real part) is as shown in Fig. 9, exponentially increases as the sweep frequency increases. A plot of the imaginary part (Nyquist plot) of the impedance against its real part are quadratic, for all the BLs, thereby confirming the symmetric nature of the carrier densities as expressed therein.

4.4 Quantum Efficiency Measurement

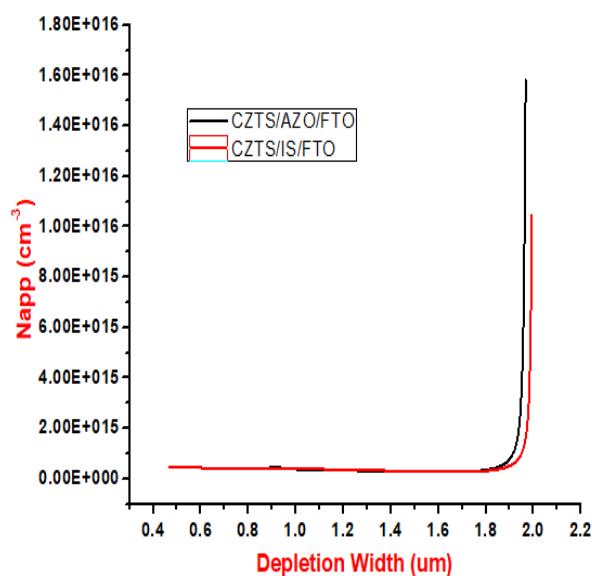
Photons with incident energy, which is of less magnitude compared with the forbidden gap of the absorber layer (CZTS) in the solar cell cannot create electron-hole pair. However, incident photons with greater energy compared to the forbidden gap produce carriers that dissipate much of their energy as heat energy.

The AZO and IS has relatively large band gaps which make them transparent to light while PVKT has a small band gap. The purpose of the TCO is to reduce the number of surface states, hence reduces surface recombination velocity at the BLs.

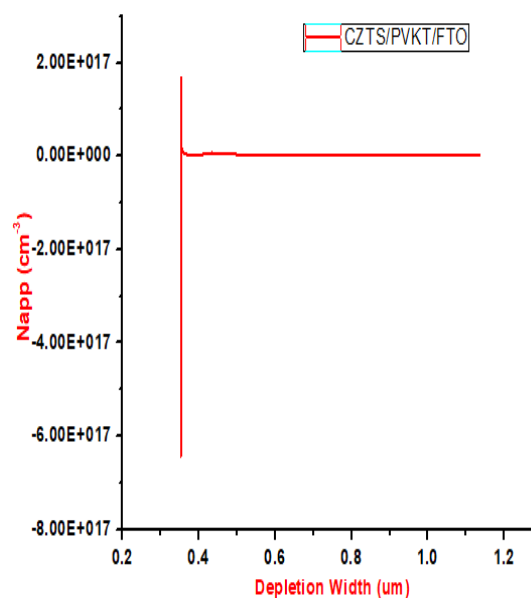
Quantum efficiency (QE) is the fragment of the excited carriers that combine in a radiative manner to the total recombination. The QE plot (Fig. 11) against the wavelength which showed that close to 90 % of the wavelength between 300 nm and 800 nm recombine in a radiative way while close to 10 % of such wavelength recombined through other processes (such as Auger and Shockely, Read, Hall (SRH) recombination) as shown in Fig. 10, for both AZO and IS BLs. The PVKT BL, according to Fig. 11, showed that less than 20 % of the wavelength between 300 nm and 800 nm recombine in a radiative way while more than 80 % of such wavelength recombined through other processes as well.

5.0 Conclusion

The basic parameters other than the J-V characteristic selected from the device simulation can be generally used in the fabrication of the solar cell. The Capacitance spectroscopy of the solar cell showed that anisotype heterojunction could be manipulated to make use of the voltage reliance on junction capacitance when the need to electronically vary it arises.

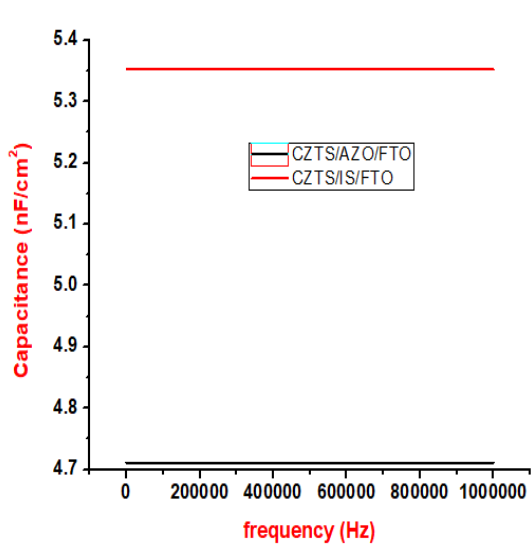


(a)

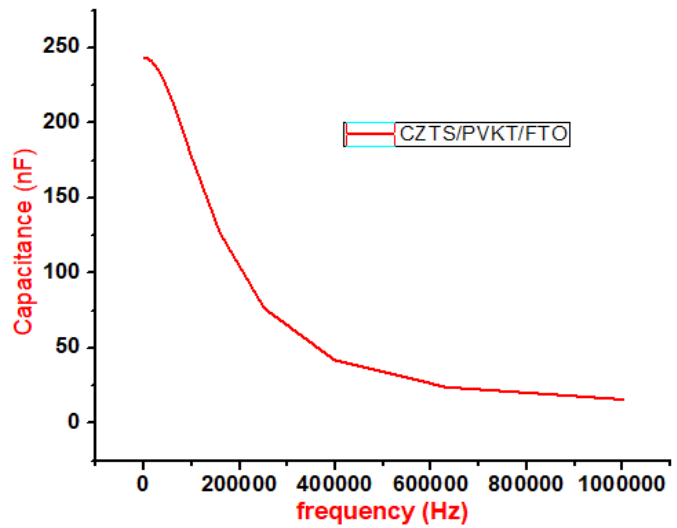


(b)

Fig. 7. Doping profile of CZTS with different BLs.

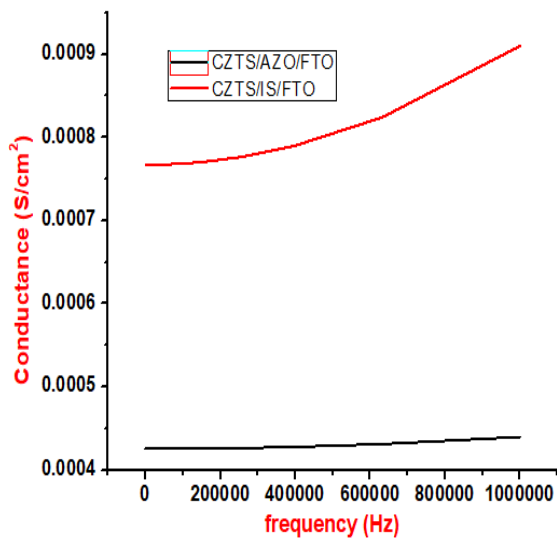


(a)

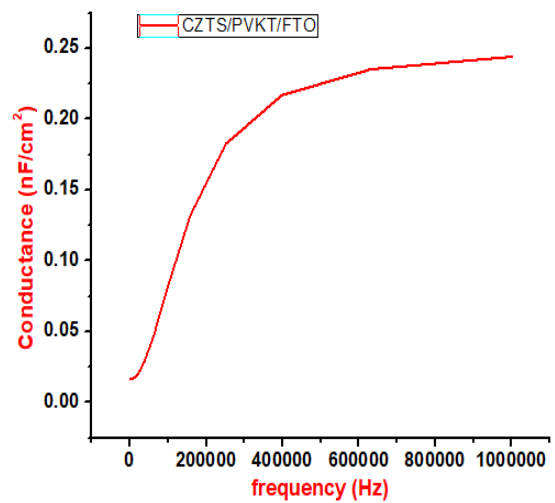


(b)

Fig. 8. Capacitance – frequency profiling of CZTS with different BLs



(a)



(b)

Fig. 9. Conductance – frequency profiling of CZTS with different BLs

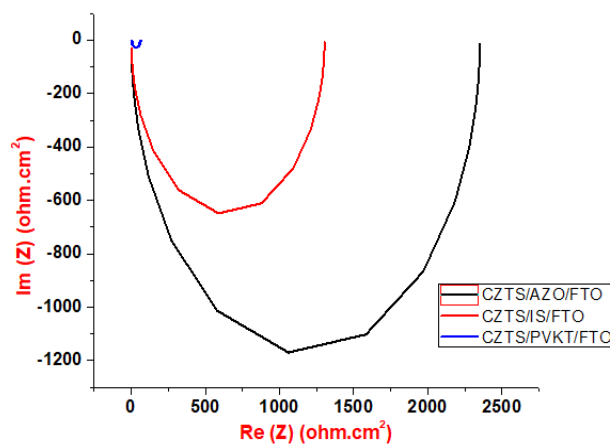


Fig. 10. Nyquist plot profiling of CZTS with different BLs

The variation of capacitance – frequency [13] enabled the evolution of the capacitance and effects according to the vibrations of AC currents. The ratio of radiative recombination to total recombination processes were so low for all the BLs at wavelength beyond the red region of visible light spectrum. The planar configuration was adopted to make the simulation easy with SCAPS-1D.

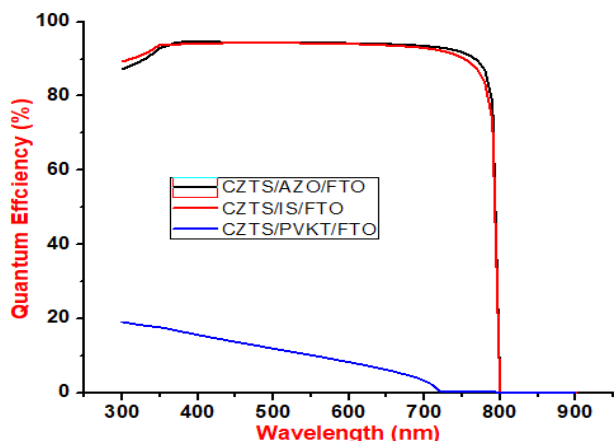


Fig. 11. Quantum Efficiency profiling of CZTS with different BLs

Acknowledgement

We are grateful to Mac Bulgeman and his co researchers at University of Gents for making SCAPS-1D available to us for use.

References

[1] Wang, K., Gunawan, O., Todorov, T., et al., “Thermally Evaporated $\text{Cu}_2\text{ZnSnS}_4$ Solar Cell,” *Appl. Phys. Lett.*, Vol. 97, pp. 143-508 2010.

[2] Rajeshmon, V. G., Poornima, N., Sudha, K. C., et al., “Modification of the Optoelectronic Properties of Sprayed In_2S_3 Thin Films by Indium Diffusion for Application as Buffer Layer in CZTS Based Solar Cell,” *J. Alloys Comp*, Vol. 553, pp. 239244 2013.

[3] Peijie Lin, Lingyan Lin, Jinling Yu, Shuying Cheng, Peimin Lu and Qiao Zheng, “Numerical Simulation of $\text{Cu}_2\text{ZnSnS}_4$ Based Solar cells with In_2S_3 Buffer Layers by SCAPS-1D”. *Journal of Applied Science and Engineering*, Vol. 17, No. 4, pp. 383-390 2014.

[4] Akinrinola Olusola., Ibiyemi A.A., Awodugba Ayodeji O and Faremi Abass A., “Numerical simulation of CZTS/ZnO/FTO hetero-junction solar cell”, *FUOYE Journal of Pure and Applied Science*. 2(1), pp 209 – 216, 2017.

[5] Takashi Minemoto and Masashi Murata, “Device modelling of perovskite solar cell based on structural similarity with thin film inorganic semiconductor solar cells”, *Journal of Applied Physics* 116, pp. 054-505, 2014.

[6] N.H. Rafat, A.M. Abdel Haleem and S.E. –D. Habib, “Numerical simulation of the limiting efficiency of the graded bandgap solar cell”, *Renewable Energy* Vol. 32, pp. 21 -34, 2007.

[7] S.M. Sze, *Physics of Semiconductor Devices*, 2nd ed. John Wiley and Sons Inc. 1981. ISBN: O – 471 – 09837 – X pp.

[8] Saïdou Madougou, Mohamadou Kaka and Gregoire Sissoko, “Silicon Solar Cells: Recombination and Electrical Parameters”, *Solar Energy*, Radu D Rugescu, IntechOpen, February 2010.

[9] B.L Theraja and A.K. Theraja, *A Textbook of Electrical Technology*. 1999 Reprint. S. Chand and Company Ltd. 1999 ISBN: 81-219-0289-4 pp.

[10] Gloeckler M., Fahrenbruch, A. L, and Sites J.R., “Numerical modelling of CIGS and CdTe Solar cells: setting the baseline”, *3rd World Conference on Photovoltaic Energy Conversion*, pp. 491 – 494, 2003.

[11] J. Tersoff, "Theory of semiconductor heterojunctions: The role of quantum dipoles", *Physical Review*, Vol. 30 (8) pp. 48-74, 1984.

[12] Pallab Bhattacharya, *Semiconductor Optoelectronic Devices*, Prentice Hall, ISBN 0-13-495656-7 1997, pp.

[13] Marc Burgelman, Johan Verschraegen, Stefan Degraeve and Peter Nollet, “Modelling Thin-film PV Devices”, *Prog. Photovolt: Res. Appl.*, ; Vol. 11, pp. 1 – 11, 2003.